Biomaterials Advances 148 (2023) 213370

Contents lists available at ScienceDirect

Biomaterials Advances

journal homepage: www.journals.elsevier.com/materials-science-and-engineering-c

Fibronectin matrix assembly and TGFβ1 presentation for chondrogenesis of patient derived pericytes for microtia repair

Hannah Donnelly [a,*], Alina Kurjan [a], Li Yenn Yong [b], Yinbo Xiao [a], Leandro Lemgruber [c], Christopher West [b], Manuel Salmeron-Sanchez [d], Matthew J. Dalby [a]

[a] Centre for the Cellular Microenvironment, Institute of Molecular, Cell & Systems Biology, College of Medical, Veterinary and Life Sciences, Joseph Black Building, University of Glasgow, Glasgow G12 8QQ, United Kingdom
[b] MRC Centre for Regenerative Medicine, The University of Edinburgh, Edinburgh EH16 4UU, United Kingdom
[c] Glasgow Imaging Facility, Institute of Infection, Immunity and Inflammation, College of Medical, Veterinary and Life Sciences, University of Glasgow, Glasgow G12 8TA, United Kingdom
[d] Centre for the Cellular Microenvironment, Division of Biomedical Engineering, School of Engineering, University of Glasgow, Glasgow G12 8QQ, United Kingdom

ARTICLE INFO

Keywords:
Microtia
Chondrogenesis
Ear tissue engineering
Ear reconstruction
Cartilage tissue engineering

ABSTRACT

Tissue engineered cartilage for external ear reconstruction of congenital deformities, such as microtia or resulting from trauma, remains a significant challenge for plastic and reconstructive surgeons. Current strategies involve harvesting autologous costal cartilage or expanding autologous chondrocytes *ex vivo*. However, these procedures often lead to donor site morbidity and a cell source with limited expansion capacity. Stromal stem cells such as perivascular stem cells (pericytes) offer an attractive alternative cell source, as they can be isolated from many human tissues, readily expanded *in vitro* and possess chondrogenic differentiation potential. Here, we successfully isolate CD146+ pericytes from the microtia remnant from patients undergoing reconstructive surgery (Microtia pericytes; MPs). Then we investigate their chondrogenic potential using the polymer poly(ethyl acrylate) (PEA) to unfold the extracellular matrix protein fibronectin (FN). FN unfolding exposes key growth factor (GF) and integrin binding sites on the molecule, allowing tethering of the chondrogenic GF transforming growth factor beta 1 (TGFβ1). This system leads to solid-phase, matrix-bound, GF presentation in a more physiological-like manner than that of typical chondrogenic induction media (CM) formulations that tend to lead to off-target effects. This simple and controlled material-based approach demonstrates similar chondrogenic potential to CM, while minimising proclivity toward hypertrophy, without the need for complex induction media formulations.

1. Introduction

Microtia is a congenital deformity of the external ear that occurs with degrees of severity. Malformation ranges from complex craniofacial deformities where ears are virtually absent, to ones that are correctly formed but smaller than usual [1]. This condition affects 1 in 6000 infants born in the UK annually [1]. Currently, microtia patients are limited in their therapeutic options. The gold standard method for external ear reconstruction to treat microtia is autologous reconstruction using costal cartilage [1,2]. This is a complex technique employed by relatively few, highly specialised, surgeons. There are, however, complications associated with creation of a secondary surgical site, with significant donor site morbidity [1,2], and challenges in producing auricles with acceptable aesthetic results [3,4].

The normal external ear is a complex three-dimensional structure, and as such, its reconstruction from cartilaginous grafts is challenging. Human ear-shaped grafts have been engineered that successfully replicate the delicate structures and mechanical strength of the native auricle [5–13]. However, most of these studies rely on costal chondrocytes as the cell source, which alongside donor site morbidity, are also hindered by limited expansion *ex vivo* [14,15]. Chondrocytes rapidly dedifferentiate in culture, and around 150–200 million cells are required for an ear-shaped graft [12,16], rendering these chondrocytes a restrictive source for regenerating full human-ear-shaped grafts. Many studies have now isolated chondrocytes from microtia tissues, although this source is minimally invasive, these cells also rapidly dedifferentiate, produce low

* Corresponding author.
E-mail address: Hannah.Donnelly@glasgow.ac.uk (H. Donnelly).

https://doi.org/10.1016/j.bioadv.2023.213370
Received 13 September 2022; Received in revised form 10 February 2023; Accepted 3 March 2023
Available online 8 March 2023

cell yields and have been reported to display different gene expression profiles from normal chondrocytes [12,17]. Acquiring sufficient chondrocyte numbers has been achieved, but involves prolonged micromass expansion, leading to chondrocytes in pellet form that are more suitable for autologous cartilage implantation (ACI)-based applications [18–21].

Bone marrow mesenchymal stromal cells (MSCs) have also been investigated as a cell source due to their chondrogenic potential and ability to expand *ex vivo* [22]. Indeed, chondrogenic induction of MSCs is well reported [23]. However, subcutaneously implanted chondrogenically induced MSCs are prone to ectopic ossification [24,25]. This is thought to be in part due to standard non-adherent micromass pellet culture lacking aspects of the *in vivo* chondrogenic niche [12]. Such high-density pellet culture encourages chondrocyte condensation and thus maturation [23]. Yet, this also minimises interactions with any physical and functional chondrogenic-niche like environmental factors - such as extracellular matrix (ECM) proteins and growth factors (GF) [26].

Typically, complex media formulations containing multiple components are employed to stimulate differentiation of MSCs down desired lineages. However, these formulations vary in potency and often lead to off-target effects [27]. For example, MSCs are stimulated to undergo chondrogenic differentiation using chondrogenic media (CM), which typically contains a cocktail of dexamethasone, ascorbate-2-phosphate and transforming growth factor beta 1 (TGFβ1). Notably, dexamethasone is also a major component of osteogenic media [27]. Using these mediums, MSC-derived cartilage has the proclivity to undergo hypertrophic differentiation [23,28]. Hypertrophy closely resembles endochondral ossification – a cartilage precursor before matrix mineralization and ossification [29].

Perivascular stem cells, or pericytes, are stromal stem cells with chondrogenic capacity [30–32]. Pericytes may offer a viable alternative stem cell source for cartilage generation, in that they have been isolated from many tissues in the body and are amenable to *in vitro* culture and expansion [30]. Pericytes are an attractive cell source as they are isolated based on a specific set of markers, based primarily on positive expression of CD146 [30]; by contrast, MSC isolation is heterogeneous, with different isolation strategies generating different lineage potentials [33,34]. This leads to a well-defined pericyte population that can be readily expanded compared to MSCs, which tend to reach senescence or differentiate to fibroblasts in culture at earlier passages [35]. As such, CD146+ pericytes isolated from microtia tissues may offer a potential high yield cell source for chondrogenic tissue generation.

Alongside investigations into an appropriate cellular source, the need for a chondrogenic graft that retains shape and mechanical properties of the ear has led to the development of biomaterial scaffolds [4,5,7,10,11,36–38]. In conjunction with computer-assisted design/computer-aided manufacturing (CAD/CAM) technology, this offers the ability to design patient-specific prosthetics that better recapitulate the complexity and structure of the ear [39,40]. However, currently used frames are non-absorbable, such as silicone or high-density polyethylene (*e.g.* Medpor®, Stryker, USA), and although they generate excellent ear shape, they lack bioactivity and are associated with infection and extrusion of the scaffold [1,2,37,38,41]. Hence, there is a need to develop bioactive scaffolds that recapitulate aspects of the native auricular chondrocyte niche and reduce risks of bio-incompatibility.

In this study we aim to address the issues of (1) development of a bioactive scaffold that mimics aspects of a chondrogenic microenvironment; (2) obtaining a clinically relevant cell source for auricular cartilage regeneration. In this regard, we have isolated CD146+ pericytes from the perichondrium vasculature of the microtia remnants (microtia pericytes; MPs) and cultured them in a chondrogenic targeting microenvironment. We have adapted a system previously used for bone repair, to present the chondrogenic-promoting growth factor (GF) TGFβ1 in a physiological manner to MPs [36,37].

This system is based on the ability of the polymer poly(ethyl acrylate) (PEA) to drive fibrillogenesis and matrix formation of the ECM protein fibronectin (FN), and permit ECM-based, solid-state delivery of ultra-low (nano) doses of GFs to cells, potentially reducing off-target effects associated with complex CM formulations [36–38]. Utilizing plasma polymerisation, PEA can readily coat 2D and 3D structures [37]. Here, we explored the PEA FN TGFβ1 system's ability to drive chondrogenic differentiation of MPs *in vitro*, in standard, high density, cell culture in 2D. However, it is easily envisioned that this technology could be applied to complex 3D systems.

2. Results

2.1. PEA drives unfolding of FN

Standard chondrogenic culture uses complex media formulations containing several soluble compounds, including the growth factor TGFβ1. Several of these compounds are also used in osteogenic media, which can lead to off-target signalling and likely the promotion of the undesired hypertrophic cartilage phenotype. In this study, we aimed to engineer a supplement-free chondrogenic promoting environment using technology previously developed, where we coat standard tissue culture plastic (TCP) with the polymer PEA by plasma polymerisation. The chemistry of PEA was confirmed using X-ray photoelectron spectroscopy (XPS) (Fig. 1A). The carbon (C1s) and oxygen (O1s) spectra show peak positioning and binding ratios similar to those found in the literature [37,39–41]. C1s spectra were peak fitted with respect to the primary hydrocarbon backbone signal at 285 eV the other three carbon moieties respectively: C-COOR (+ 0.4 eV); C—O (+ 1.8 eV); O-C=O (+ 3.4 eV), corresponding to chemical structure inset in Fig. 1A. In O1s spectra two oxygen moieties, C=O (~532 eV) and C-O-C (~533 eV) were found. Thus, these XPS results confirm the successful coating of PEA onto substrates by plasma polymerisation. As previously described, fine-tuning of the parameters of the plasma system, such as chamber pressure, power, and polymerisation time, enables PEA coatings onto TCP substrates at a rate of 10 nm min^{-1} [37,39]. The thickness of the resultant PEA coatings (≈300 nm) guarantees that the XPS spectra are due to PEA and not to the underlying substrate, as the sensitivity of XPS is ≈10 nm [37,39,40].

Our previous work has demonstrated that PEA is able to drive fibrillogenesis and matrix formation of FN [36–38]. To confirm this, FN was adsorbed onto PEA and TCP surfaces, atomic force microscopy (AFM) analysis shows the polymer PEA drives cell-free network formation of FN (Fig. 1B). TCP is used as a control and shows FN molecules remain in a globular formation. Unfolding of FN molecules leads to exposure of cryptic binding domains, such as an integrin and GF binding domain (Fig. 1C). Immunofluorescence analysis was used to demonstrate a similar amount of total FN was adsorbed onto TCP and PEA, but FN unfolding on PEA led to significantly increased availability of the P5F3 (GF binding) and HFN7.1 (RGD integrin binding) domains (Fig. 1D). The scheme in Fig. 1E demonstrates FN conformation upon adsorption to TCP (globular, binding sites inaccessible) and PEA (unfolded network, binding sites exposed).

It is well reported that the GF binding domain of FN has high affinities for many GFs[42], including the chondrogenic GF TGFβ1 [43,44]. As previously demonstrated with the osteogenic GF BMP-2 [36,37,45], TGFβ1 was adsorbed to the PEA-driven FN matrix to present the GF in a solid-phase, physiological-like manner to cells. We hypothesised the PEA FN TGFβ1 system may enhance chondrogenesis in cells seeded to these surfaces.

2.2. Isolation of pericytes from microtia patient biopsies

Pericytes are stromal stem cells that have been isolated from many different tissues, and display osteogenic, chondrogenic, adipogenic and myogenic potential in culture [30]. Here, we investigated pericyte isolation from a novel tissue, the perichondrium of the microtia remnant, with the aim that these cells may offer a potentially autologous

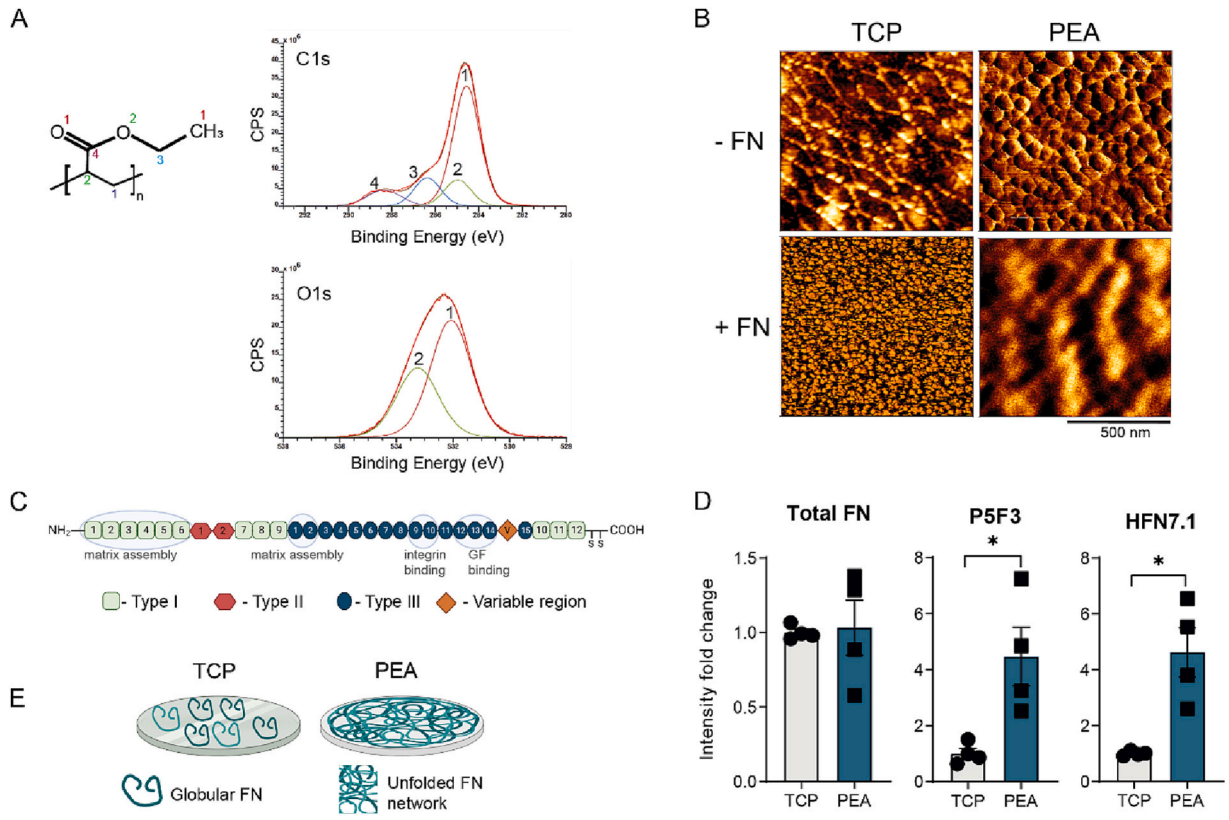

Fig. 1. PEA drives exposure of FN binding domains. A. Chemical composition of the plasma polymerised PEA surface measured by XPS analysis. C1s and O1s core-level spectra of PEA with fitted peaks which represent binding conformations of carbon and oxygen atoms on the top 10 nm of the sample surfaces. The inset show's chemical structure of PEA, with labelled carbon and oxygen atoms corresponding to components as indicated on C1s and O1s scans. The spectra show similar peak positioning and binding ratios to those previously described [42,44,46]. B. AFM images of FN adsorbed (20 μg/mL) onto TCP and PEA surfaces demonstrates FN unfolding on PEA, whereas on TCP, FN appears to remain in a globular formation. C. Schematic of fibronectin molecule, demonstrating proximity of GF and integrin binding domains. D. Domain availability of adsorbed FN. Immunofluorescence analysis demonstrates total FN availability shows no significant differences between PEA and TCP, suggesting equal amounts are adsorbed. Functional FN domains, P5F3 (GF-binding domain) availability and HFN7.1 (RGD integrin-binding domain), that are concealed in globular FN molecules, show increased availability on PEA. Graphs show mean ± SEM, using unpaired two-tailed *t*-test with Mann-Whitney*$p < 0.05$, $n = 4$ material replicates. E. Schematic demonstrates FN remains globular on TCP and unfolds to form a network on PEA. C and E created with BioRender.com.

chondrogenic cell source for ear reconstruction for microtia patients. Cells surrounding the vasculature from the tissue biopsy (Fig. 2A) demonstrated co-expression of pericyte markers CD146 and α-SMA (α-smooth muscle actin) (Fig. 2B). Ear tissue was digested as previously described [30] and MPs were isolated using FACS based on well-validated pericyte markers (CD146+ CD34- CD31- CD45-) (Fig. 2C). These cells were morphologically similar to pericytes isolated from other sources [30] (Fig. 2D). MPs retained the CD146+ phenotype up to passage 8 (Supplementary Fig. 1). MPs were successfully isolated from the tissue of 10 different patients, providing a viable cell source for this research (data not shown).

2.3. PEA FN with matrix-bound TGFβ1 leads to GFR and FA co-localisation

Synergy signalling between co-localised GF receptors (GFR) and integrins has been shown to enhance lineage commitment in MSCs [46,47]. Due to the close proximity of the integrin and GF binding site presented to cells on PEA FN networks (Fig. 1C-E), we wanted to investigate whether PEA FN surfaces binding adsorbed TGFβ1 led to co-localisation of TGFβRs and FAs. TGFβ1 was adsorbed in solution at 100 ng/mL to FN coated PEA surfaces to present the GF in solid-phase to the cells (bound), PEA FN TGFβ1 surfaces were then washed with PBS to remove any excess, unbound GF. We compared this to PEA FN surfaces with TGFβ1 administered soluble in the culture media (soluble). MPs were seeded on PEA FN TGFβ1 soluble and bound substrates, and after 4 h of culture, cells were fixed and imaged using super-resolution microscopy. Representative images of PEA FN TGFβ1 (bound) are shown in Fig. 2A and Supplementary Fig. 2b (representative images for PEA FN + soluble TGFβ1 in Supplementary Fig. 2A). We measured the average distance between TGFβR and focal adhesions (FAs), represented by vinculin staining. Here we found matrix bound TGFβ1 leads to a significantly shorter distance on average between the GF receptors and FAs (Fig. 3B). This suggests co-localisation of TGFβR to FAs is enhanced when TGFβ1 is bound on the PEA FN surface.

2.4. Matrix-bound TGFβ1 supports SOX9 expression

To investigate if PEA FN with matrix bound TGFβ1 (PEA FN TGFβ1) could support chondrogenesis of MPs, we compared the system to MPs seeded in CM (Fig. 4A). MPs were seeded onto PEA FN TGFβ1 and PEA FN substrates, TCP (standard media; negative control), TCP + CM (positive control). As chondrocytes typically live in pairs [23], MPs were seeded in high density culture (HDC) for 7 and 21 days. Light microscopy images of HDC on substrates revealed significant differences in bulk culture morphology (Fig. 4B). On the TCP control, by 7 days of culture, cells had begun to aggregate, and cell layers peeled from the TCP surface. In CM, cell aggregates appeared by day 7, and by day 21 were visible by eye and had begun to detach from the substrate surface. By contrast, on PEA FN TGFβ1 substrates, cells appeared to resist peeling

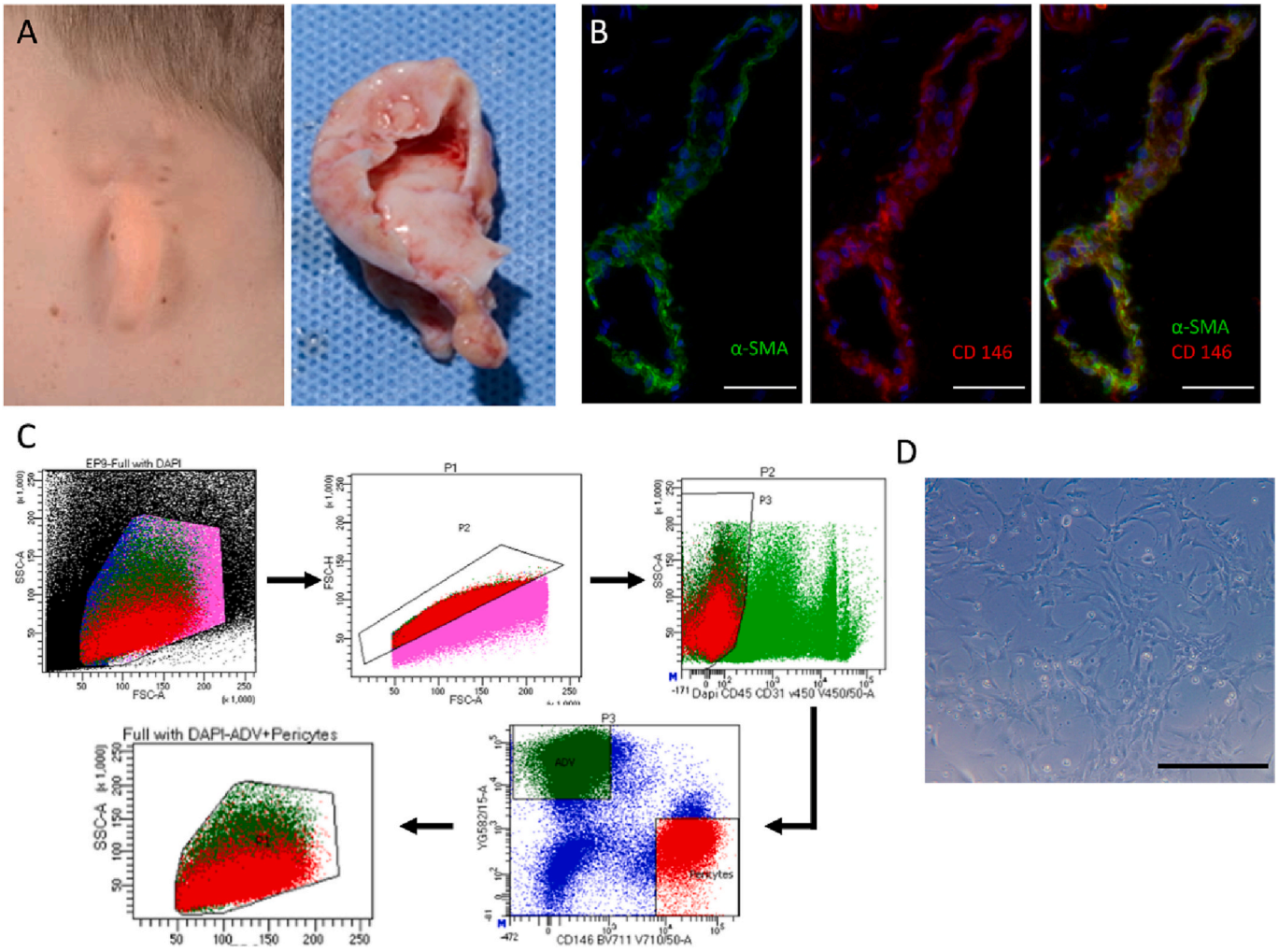

Fig. 2. Isolation of pericytes from microtia remnants. **A**. Lateral photograph of patient with grade III microtia and complete external auditory canal atresia as well as the microtia remnant **B.** Immunofluorescence images of intact microtia tissue, stained for pericyte markers α-SMA and CD146, displaying positive expression around vasculature**,** scale bar 50 μm. Blue; nuclear staining. **C.** FACS plots of microtia pericyte (MP) isolation. Tissue was digested and forward scatter area (FSC-A) *versus* side scatter area (SSC-A) plot used to identify single cells; following removal of dead cells (DAPI), haematopoietic cells (CD45) and endothelial cells (CD31), pericytes can then be identified as CD146+ and CD34- and Adventitial cells (ADV) as CD34- CD146+ **D.** Light microscopy image of MPs in standard culture at passage 6, scale bar 200 μm.

and aggregation, instead forming dense sheets of cells over the substrate surface. We note that it is thought for implant coating, cell sheets, rather than cell aggregates, are thought to be more desirable [6].

At days 7 and 21, samples were fixed to assess early and late chondrogenic markers, SOX9 and COL2, by immunofluorescent staining. By day 7, SOX9 expression was significantly increased in the PEA FN TGFβ1 condition (Fig. 4C). As SOX9 is the master transcriptional regulator of the chondrogenic response [23], this suggests the PEA FN TGFβ1 substrate may be promoting early chondrogenesis in MPs. By day 21, CM was the only condition to significantly increase collagen type II levels above the TCP control. However, all samples demonstrated positive collagen type II expression (Fig. 4D).

2.5. Late chondrogenic marker expression

MPs were harvested from controls and substrates at 21 days for RNA analysis. PEA FN TGFβ1 significantly down regulated the hypertrophy marker alkaline phosphatase (ALP), while CM significantly upregulated the expression of the mature chondrocyte marker COL2A (Fig. 5A), consistent with the immunofluorescence analysis (Fig. 4D). Although the expression of COLX did not appear to be significantly changed in any of the conditions compared to the TCP control, expression of COL2A/COLX suggests collagen expression in CM is slightly skewed toward COL X, suggestive of hypertrophic chondrocytes (Fig. 5A). Safranin-O histological staining revealed both PEA FN TGFβ1 and CM comparably support chondrogenesis compared to TCP and PEA FN controls (Fig. 5B).

2.6. Regulation of SMAD signalling

SMADs (small mothers against decapentaplegic) are intracellular mediators activated by phosphorylation upon TGFβ1/SMAD signalling [48,49]. TGFβ1 ligand binding leads to the phosphorylation and activation of SMADs 2 and 3, which, upon translocation to the nucleus, induce expression of cartilage associated genes - type II collagens, aggrecans and SOX9 [49]. Whereas SMADs 1 and 5 are commonly activated by bone morphogenetic protein-2 (BMP-2) ligand binding and induce the transcription of genes that are associated with the hypertrophic phenotype, ALP and collagen X [50]. Expression levels of total SMADs and phosphorylated SMADs were investigated by western blotting after 7 days. CM led to increase in levels of pSMAD2, but also of total SMAD1 levels (Fig. 6A,B, Supplementary Fig. 3). Interestingly, however, only low levels of all SMADs and pSMADs were detected in MPs cultured on PEA FN TGFβ1 by western blotting.

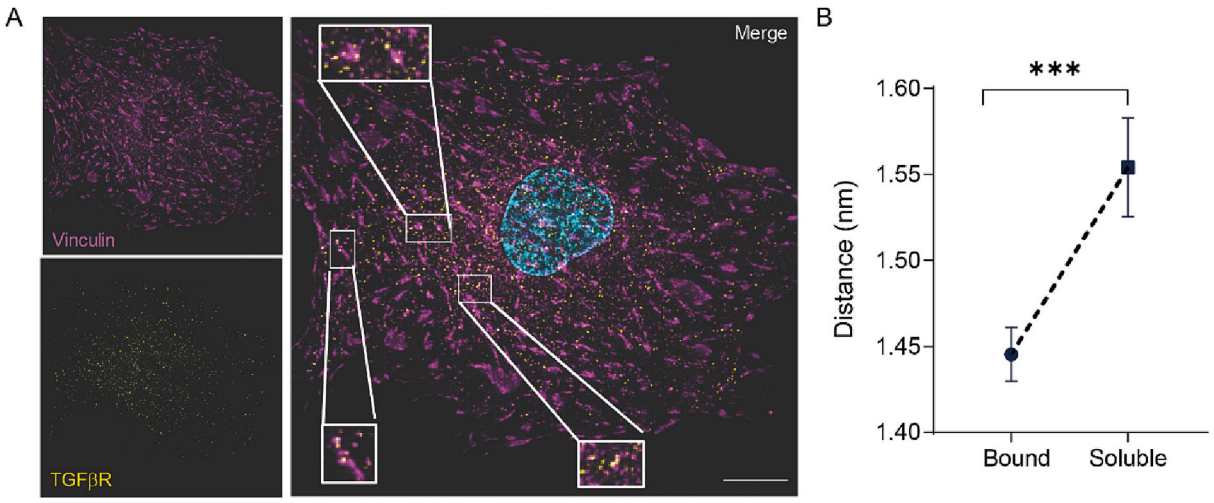

Fig. 3. TGFβ1 adsorbed to the PEA FN system leads to co-localisation of TGFβ1 to focal adhesions. A. Representative super-resolution image of MPs seeded on PEA FN TGFβ1 surface, demonstrates co-localization of TGFβR (yellow) to focal adhesions (vinculin; magenta), white boxes show magnified regions of co-localization. Cyan; nuclear staining. Scale bar is 10 μm. B. The distance of TGFβR to focal adhesions (FAs, vinculin) was measured in cells cultured on PEA FN with matrix bound TGFβ1 (PEA FN + adsorbed TGFβ1; bound) and TGFβ1 administered soluble in the culture medium (soluble). TGFβ1 is significantly closer to FAs when TGFβ1 is matrix bound (bound; PEA FN TGFβ1), graph shows mean ± SEM of distance of ≥1500 particles measured, $n = 3$ material replicates, significance calculated using unpaired *t*-test,***$p < 0.0005$.

3. Discussion

One of the major challenges associated with the clinical translation of engineered human-ear cartilage is the lack of a clinically applicable cell source. The ideal cell source should possess chondrogenic potential, lack proclivity for ossification, avoid donor site morbidity and produce the high cell yields required for entire auricular reconstruction. Approximately 100× more cells are required than for ACI procedures, typically used to treat articular cartilage defects in the knee [51]. Native, autologous, chondrocytes either sourced either from a secondary site or from microtia tissue biopsies demonstrate strong chondrogenic potential [12,15]. However, chondrocytes dedifferentiate in culture quickly, rendering their *in vitro* expansion ineffective.

This has led many studies to investigate the co-culture of chondrocytes cultured with MSCs [12,13,51,52]. MSCs are able to produce the high cell yields required, yet chondrogenic stimulation using current methods, such as CM, often leads to undesired effects such as hypertrophy or ossification upon implantation *in vivo* [23–25,28]. Further, the MSCs used in many of these studies are bone marrow derived, and although relatively non-invasive, for an autologous therapy this would require a secondary procedure. In this study we successfully isolated CD146+ pericytes from microtia patients from a piece of tissue that would otherwise be discarded. These multipotent cells have the advantages of availability, defined phenotype and enhanced expansion capability [30]. We envisioned isolating MPs from chondrogenic tissues may have positive influence on their chondrogenic potential, as has been reported for osteogenesis of BM-derived MSCs [34]. MPs offer a viable cell source for the high yield of cells required for auricular reconstruction as they can be readily expanded *in vitro* up to passage 8 without loss of CD146 expression, *i.e.* without loss of stemness/differentiation capacity (Supplementary Fig. 1). This is consistent with pericytes isolated from other tissues, such as muscle, which have been demonstrated to retain proliferation capacity and CD146+ NG2+ expression up to passage 14 [30].

A recent study isolated adipose-derived MSCs from the microtia remnant and demonstrated their chondrogenic potential, then by expanding and culturing with microtia chondrocytes, costal chondrocytes and adipose-derived costal MSCs they successfully implanted a 3D printed ear shaped graft in a murine model [13]. Future work could similarly investigate the PEA FN TGFβ1 with co-cultures of MPs and chondrocytes isolated from microtia biopsies, as co-cultures with chondrocytes even in low numbers, may further mimic functional aspects of a chondrogenic microenvironment and support more robust chondrogenesis of the MPs [13,28,53], while MPs may support the proliferation and stability of the microtia chondrocytes *in vitro* [13,54]. It is easily envisioned that microtia chondrocytes could be isolated from the same tissue sample as the MPs during FACS sorting. This negates the use of BM-derived MSCs and ensures both cell types can come from an autologous, minimally invasive source.

Here, we further develop a polymer-based system to present the GF TGFβ1 to cells in a physiological manner. By tethering low concentrations of TGFβ1 to open FN molecules on PEA, we demonstrate induction of chondrogenesis in MPs seeded in HDC that is comparable to chondrogenic media. The PEA system promotes co-localization of the TGFβR with focal adhesions (Fig. 3), although this did not appear to lead to an increase in total SMAD2/3 signalling by western blot (Fig. 6), suggesting lack of activation, however it also did not increase hypertrophy markers SMAD 1 or pSMAD1/5/9 levels as CM did. The significant reduction in ALP gene expression further suggests this system may potentially reduce the proclivity of cells for ossification. Future work will optimise concentrations of TGFβ1 used in the system and then further investigate TGFβ activation and downstream signalling at different time points, to understand if the system can be used to promote robust SMAD2/3 activation.

In conclusion, the PEA FN TGFβ1 substrate was seen to increase SOX9 expression in MPs, key to initiation of chondrogenic differentiation [23]. While it did not strongly increase SMAD 2 or 3 that are relevant to hyaline phenotype [49], it also did not induce SMAD 1 or 5 that are implied in hypertrophy [50]. Collagen II expression was observed to be lower with PEA FN TGFβ1 than with CM, however chondrogenesis at the histological level was seen to be enhanced along with significant reduction in markers linked to hypertrophy such as ALP. Further, while CM led to the formation of large cell aggregates that peeled from the substrate, PEA FN TGFβ1 supported growth of cell sheets that could be useful in tissue engineering applications. Further, it is easily envisioned that biocomaptiable and biodegradable 3D printed ear constructs (*e.g.* [13]) could be coated with PEA FN and low dose TGFβ1 to support 3D chondrogenesis of MPs. The coating technology is facile and could be envisioned for other cartilage applications such as in provision of cells for ACI.

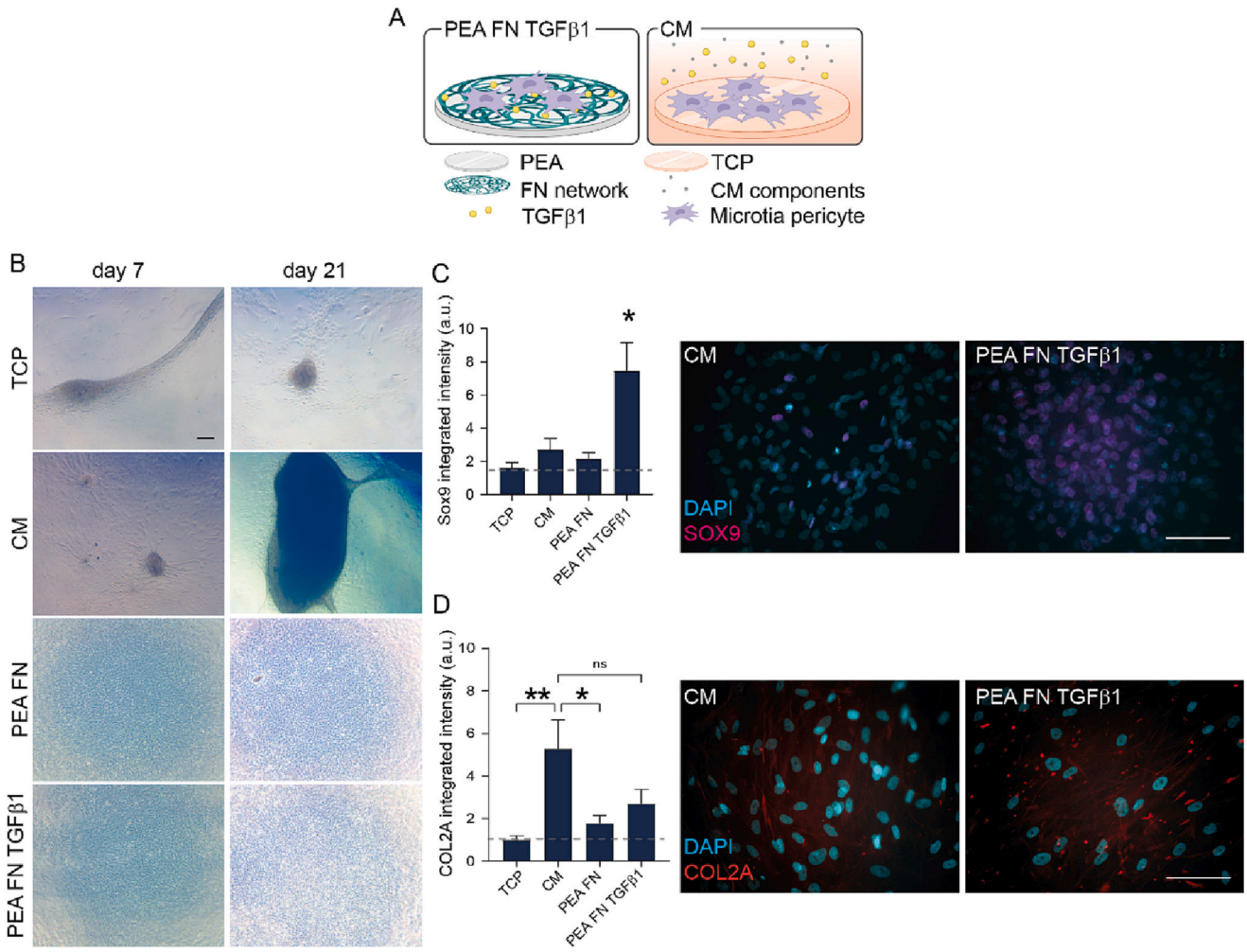

Fig. 4. MPs grown on PEA FN TGFβ1 resist aggregation and have increased SOX9 expression. A. Schematic showing culture set up for matric bound TGFβ1 on the PEA FN TGFβ1 substrate, compared to CM control containing soluble TGFβ1. Created using BioRender.com. B Light microscopy images of MPs grown on TCP, TCP CM (chondrogenic media) and PEA FN TGFβ1 at 7 and 21 days. On TCP and TCP CM, cells grow in aggregates, leading to peeling of cell layers from the culture surface. This is more pronounced in CM, which by day 21 shows large cell aggregates that can detach from the substrate surface. On PEA FN TGFβ1, high density seeding does not lead to cell aggregation or pealing but displays a high-density confluent layer covering the substrate surface. Scale bar is 200 μm, $n = 4$, representative images shown. C. Quantification of immunofluorescence images of MPs after 7 days. PEA FN TGFβ1 significantly upregulates SOX9 levels. Scale bar is 100 μm, n = 4, cyan; DAPI, Magenta; SOX9. D. COL2a expression was observed in all samples at day 21. CM significantly elevated expression compared to TCP control. Scale bar is 100 μm, n = 4 material replicates, cyan; DAPI, red; COL2A. C and D measured by SOX9/COL2A frame integrated intensity/number of nuclei; results are mean ± SEM, n = 4 material replicates, significance calculated using one-way ANOVA with Tukey multiple comparisons test, ns = non-significant, $^{**}p < 0.005$, $^{*}p < 0.005$.

4. Methods

4.1. Preparation of substrates

Circular 12 mm diameter Nunc™ Thermanox™ coverslips were subject to plasma polymerisation with ethyl acrylate (Sigma Aldrich). Plasma polymerisation was carried out in a custom-made capacitively coupled plamsa installation for low-pressure plasma in a 15 L T-shaped reactor made of borosilicate and stainless steel end plates sealed with Viton O-rings. Under vacuum, the plasma was initiated *via* two capacitively coupled copper band ring electrodes situated outside of the reactor chamber and connected to a radio frequency power supply (Coaxial Power System LTD.). Samples were treated for 10 mins at 100 W. Creating a PEA coating, of around 300 μm[42]. PEA coated coverslips were placed on parafilm and FN from human plasma (Sigma Aldrich) adsorbed in solution (20 μg/mL) and incubated at RT for 1 h. Substrates were then washed twice with PBS and TGFβ1 (Peprotech) added in solution (100 ng/mL) and incubated for 2 h at RT. After two washes with PBS substrates were transferred into 24-well plates in PBS until ready to use.

4.2. XPS

After plasma polymerisation, samples were sent out to the National EPSRC Users' Service (NEXUS) (http://www.ncl.ac.uk/nexus/) for X-ray photoelectron spectra (XPS) analysis. A K-alpha XPS system (ThermoScientific) equipped with a monochromatic Al K-alpha source was used to analyse each sample three times at a maximum beam size of 400 μm × 800 μm. Parameters were set up as follows: X-ray energy: 1486.68 eV; voltage 12 kV; current: 3 mA; power 36 W. Spectra analysis and curve fitting performed using CasaXPS software.

4.3. FN adsorption assays

Quantitative immunofluorescence assays were carried out using the LI-COR in-cell western™ platform. FN (20 μg/mL) was adsorbed for 1 h at RT, samples were washed with 3 × 5 min with PBS, blocked with 1 % milk protein/PBS, and incubated with primary antibodies for total FN

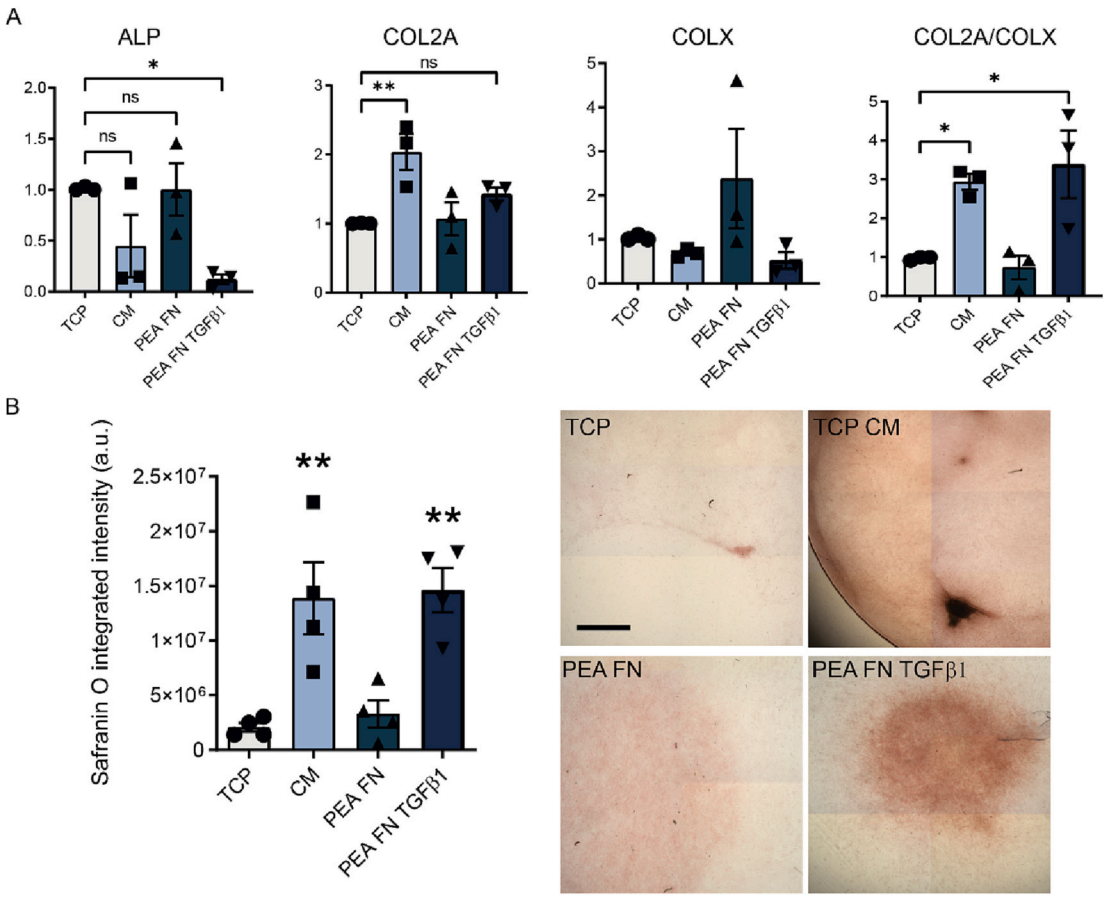

Fig. 5. PEA FN TGFβ1 supports chondrogenesis of MPs similar to CM, but reduces ALP expression. A. qRT-PCR comparison of chondrogenic and off-target gene expression at day 21 induced by CM or PEA FN TGFβ1, $n = 3$ material replicates from 3 independent experiments with different donor cells. PEA FN TGFβ1 significantly reduces ALP expression and leads to a higher ratio of COL2A to COLX. B. PEA FN TGFβ1 and CM significantly support chondrogenesis at 21 days, demonstrated by Safranin-O histological staining. Scale bar is 2 mm. Results are means ±SEM, $n = 4$ material replicates, significance calculated using one-way ANOVA with Tukey multiple comparisons test to TCP control, $^{*}p < 0.05$, $^{**}p < 0.005$, $^{***}p < 0.0005$.

(polyclonal rabbit, Sigma Aldrich), HFN7.1 (monoclonal mouse, Developmental Studies Hybridoma Bank, USA), and P5F3 (monoclonal mouse, Santa Cruz Biotechnology, sc-18,827) for 2 h. Substrates were washed 5 × 0.5 % Tween20 in PBS (PBST), followed by incubation o/n at 4 °C with LI-COR secondary antibodies (IRDye 800CW/700CW anti-rabbit/mouse secondary antibody, LI-COR, UK). Samples were washed 5× with PBST, followed by a final wash in PBS and dried before imaging on LI-COR Sa Odyssey scanner.

4.4. Pericyte isolation

Pericytes were isolated from tissue of Microtia patients undergoing the first stage reconstruction with informed consent, ethical approval for the collection, processing and subsequent research using human auricular tissue was granted by Southeast Scotland Research Ethics Committee 01 (ref [16]:/SS/0103). All subsequent methods were performed in accordance with the guidelines and regulations. The auricular perichondrium was dissected off the cartilage under loupe magnification. Perichondrial tissue was digested using Collagenase II 1 mg/mL (GIBCO) in DMEM in a 37 °C shaking water bath at 150 rpm for 2 h. Samples were vortexed every 30 min at 2.0 rpm for 30 s-1 min. 1 mL of featal bovine serum (FBS; Sigma Aldrich) was then added to neutralize collagenase. Samples were centrifuged at 2.0 rpm for 10 mins and the supernatant discarded leaving the pellet. Pellets were resuspended in 5 mL PBS/2 % (v/v) FBS. The resultant tissue suspension was then filtered through 100 μm, 70 μm and 40 μm cell strainers. The filtered solution was then made up to 30 mL and centrifuged at 2.0 rpm for 10 mins. Supernatant was discarded and pellet resuspended in PBS/2 % FBS for immunostaining. Fluorescently activated cell sorting (FACS) was carried out on cells stained with CD146 BV 711, CD34 FITC, CD31 V450, CD45 V450, final dilution 1:100, (all from BD BioSciences). Cells were stained for 45 mins at 4 °C in the dark before undergoing sorting with the BD FACS Aria II. The pericyte population was sorted based on the following phenotype CD146+, CD34-, CD45-, CD31-.

4.5. Pericyte culture

Immediately after FACS, pericytes were seeded onto 0.1 % gelatin-coated wells at a density of 2×10^4 cells/cm^2 in EGM-2 endothelial growth medium (Lonza) in a humidified incubator with 5 % CO2 at 37 °C. When confluent, cells were detached using trypsin/versene and split into uncoated wells and cultured in 20 % DMEM for all subsequent passages. Media changed twice per week and cultured until ready for use or until passage 10. During experimental culture, pericytes were seeded in micromass onto PEA substrates or TCP in 24-well plates. 1×10^5 cells were seeded onto each substrate in a total volume of 30 μL. The cells were incubated under a humidified atmosphere of 5 % CO_2 at 37 °C for 3 h to allow cell attachment, after which they were gently flooded with 1 mL of culture media. TCP, PEA FN conditions were cultured in DMEM with 10 % FBS, 2 % penicillin streptomycin, 1 % sodium pyruvate and 1 % MEM-NEAA. For PEA FN TGFβ1 this was supplemented with 10 ng/mL TGFβ1 on day 3 and for all subsequent media changes. Chondrogenic media was used for the TCP-CM condition (DMEM supplemented with 10 % FBS, 2 % penicillin streptomycin, 1 % sodium pyruvate, 1 % MEM-

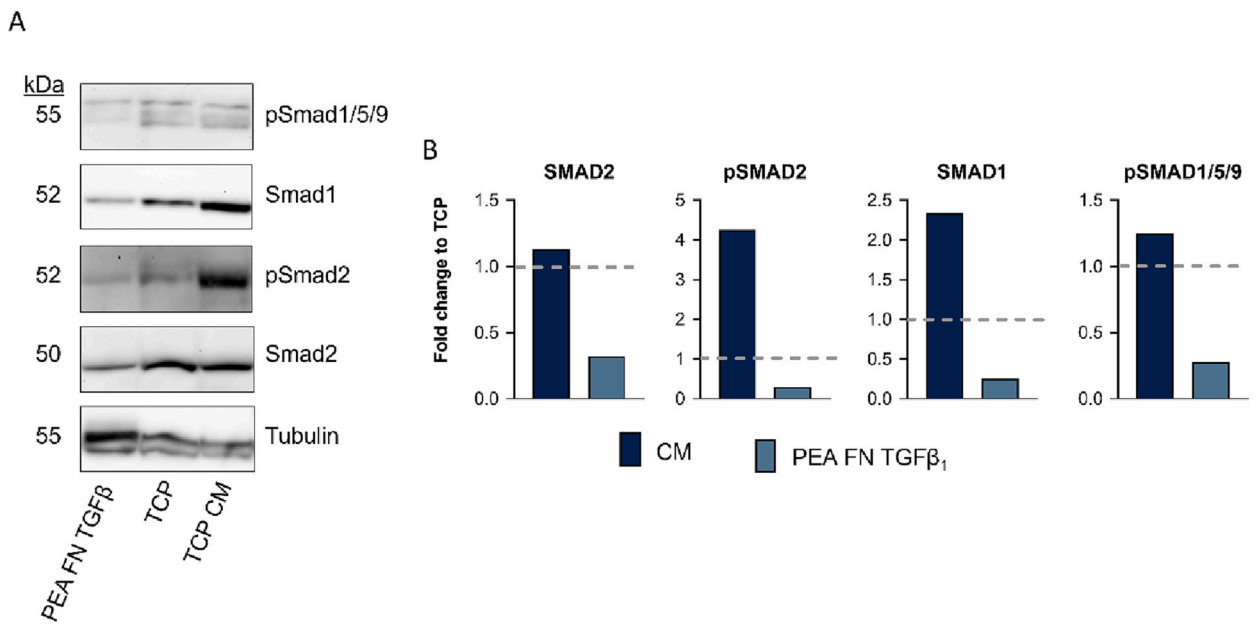

Fig. 6. SMAD signalling in MPs. A. and B. After MPs had been cultured for 7 days on TCP, CM and PEA FN TGFβ1, protein was extracted from 4 material replicates and subject to western blot analysis for SMAD signalling molecules. Each protein was run on a separate gel with the same time of exposure. Full length blots presented in Supplementary Fig. 2. B. Quantification of bands shown in A represented as fold change compared to TCP. PEA FN TGFβ1 produced only low quantities of all SMADs while CM had elevated levels of all SMADs. SMAD2 is specific to signalling to a more hyaline cartilage phenotype, (*i.e.* the desired signalling response). However, CM also led to increased levels of SMAD1 and pSMAD1/5/9, which signals through osteogenic-related pathways and is associated with the formation of hypertrophic cartilage, $n = 4$ pooled material replicates.

NEAA, 100 μM ascorbate-2-phosphate, 107 M dexamethasone, 1 % ITS (insulin 10 μg/mL, transferrin 5.5 μg/mL, selenium 6.7 ng/mL), 50 μg/mL proline, 10 ng/mL TGFβ1). 500 μL of media was removed and replaced twice per week.

4.6. Immunocytochemistry

Cells were washed 1 x PBS and fixed with 4 % formaldehyde solution at 37 °C for 15 min. Cells were then permeabilized with a solution of 0.5 % Triton X-100 in PBS at 4 °C for 5 min. 1 % BSA solution was added, cells incubated for 1 h at RT to block nonspecific binding. After blocking, primary antibodies were added, for day 7 samples (anti-SOX9, 1:250, rabbit mAb, Abcam #185966; anti-Aggrecan, 1:200, mouse mAb, Abcam #ab3778), and for 21 day samples (anti-COLII, 1:200, Abcam ab34712; anti-COLX 1:200, Abcam 49,945), and incubated at 37 °C for 1 h. Cells were then washed with 0.5 % Tween20 in PBS (PBST) 3 × 5 min. Thereafter, a biotinylated anti-rabbit secondary antibody (1:50; Vector Laboratories) were added to the cells and incubated at 37 °C for 1 h, followed by 3 × 5 min PBST washes. After washing, streptavidin-fluorescein (1:50; Vector Laboratories) was added and incubated at 4 °C for 30 min. After final 3 × 5 min PBST washing, nuclei were stained with Vectasield-DAPI (Vector Laboratories), whereas the samples were mounted on glass slides for fluorescence microscopy. Samples were then viewed on Axiophot microscope and processed using ImageJ.

For imaging of intact microtia tissue, samples were fixed in 4 % PFA overnight at 4 °C before being embedded, frozen in OCT and cryosectioned. Tissue slides were washed with PBS and antigen retrieval was performed with Tris-EDTA. Protein block was performed for 30 mins at room temperature before primary antibody incubation (1:100), CD146 (Abcam, ab75769) CD34 (Abcam, ab81289) or directly conjugated α-SMA-FITC (1:100, Sigma F3777) overnight at 4 °C. Secondary antibodies, all 1:250, AlexaFluor 488 Goat anti-rabbit (H + L) (Invitrogen), AlexaFluor 647 Goat anti-rabbit (H + L) (Invitrogen) or Streptavidin conjugated 488 (Life technologies) was applied for 30 mins at room temperature. Tissue samples were washed and mounted with DAPI containing mountant (Thermo Fisher Scientific, P36931). Images were acquired using Zeiss (Carl Zeiss, Oberkochen, Germany). Images were processed using ZEN Blue lite version (Zeiss).

4.7. Flow cytometry

Cells were detached from tissue culture flasks using TrpLE (Thermo Fischer) at passage 6 or 8. Centrifuged at 400 *g* for 4 mins, supernatant discarded and resuspended in PBS/2 % FBS +0.25 mM EDTA (FACS buffer) and centrifugation repeated to wash. Pellet was then resuspended in FACS buffer containing antibodies (1:50) against CD146 (PerCP-Cy5.5, BD Biosciences, 562,134), CD45 (FTIC, BD Biosceinces, 11–0459-42), CD34 (PE, BD Biosciences, 12–0349-42) and CD56 (PE-Cy7, BD Biosciences). After washing, cells were run on Attune™ NxT Flow Cytometer (Thermo Fischer) and analysed using FlowJo Software.

4.8. Super resolution microscopy

An Ibidi® μ-slide 8 well high glass bottom slide (80807) was plasma coated with PEA and FN was adsorbed as described above. TGFβ1 was then adsorbed onto the PEA surface or administered in soluble form in cell media (100 ng/mL). Cells were seeded and fixed after 4 h. Cells were then incubated with primary antibodies TGFBR1 (1:100, Thermo Fischer PA5–32631) and vinculin (1:400, Sigma V9264). Super-resolution structured illumination microscopy (SR-SIM) was performed using a Zeiss Elyra PS.1 super-resolution microscope (Carl Zeiss, Germany). A plan-Apochromat 63×/1.4 Oil lens was used, and *Z*-steps of 0.2 μm were acquired (total thickness between 5 and 7 μm) in five rotations using the ZEN Black Edition Imaging software. SR-SIM images were reconstructed in the same software using Structural Illumination automatic processing tool. Distance between TGFbR and vinculin was measured using Fiji with DiAna plugin measuring centre to centre [55].

4.9. Quantitative real-time PCR

RNA extraction was performed after 21-days cell culture. Cells were lysed, and total RNA extracted using a Qiagen RNeasy mini kit

(deoxyribonuclease treatment included). Quantity and integrity of RNA was measured with NanoDrop (Thermo Fischer). qPCR was carried out and analysed to assess the expression of target primers (Table 1, all from Eurofins). Briefly, RNA samples were reverse-transcribed using the QuantiTech Reverse Transcription Kit (Qiagen). qPCR was carried out using the SYBR Select Master Mix (Life Technologies) and the 7500 Real-Time PCR System (Applied Biosystems). B-ACTIN served as the housekeeping gene, and expression for the genes of interest was normalised to B-ACTIN expression. Because the SYBR green method was used, primer sequences for the genes were validated by dissociation curve/melt curve analysis. The comparative cycle threshold method was used for quantification of gene expression. The relative transcript levels were expressed as mean ± SEM (n = 4 technical replicates, for 3 patient replicates).

4.10. Histology

For ALP staining cells were fixed with 0.1 % glutaraldehyde in PBS for 20 min at RT. Rinsed 3 x PBS, rinsed 1 x with 1 % acetic acid solution for 10–15 s and stained with 0.1 % Safranin O solution (Merck) for 5 min. Cells were then washed 3 x PBS and stored in PBS. Light microscopy images obtained using Thermo Fischer EVOS M700. Integrated density measurements obtained by drying samples and scanning using LiCor Odyssey Sa system.

4.11. Western Blotting

After 7 and 21 days of culture, biological triplicates were scraped from the substrates, combined, and lysed using radioimmunoprecipitation (RIPA) buffer supplemented with phosphatase inhibitors (ThermoFisher, 78,427) and protease inhibitors (Sigma-Aldrich, S8830). The cells were kept on ice with periodical vortexing for 30 min, then centrifuged at 12,000 *g* for 15 min at 4 °C. Western blotting was performed using the same amount of protein in each sample, measured by DC assay (Biorad). Western blotting was performed using Bolt 4–12 % Bis-Tris Plus gels (Invitrogen). Gels were transferred on a membrane and blocked for 1 h using 5 % milk solution (*w/v*) in Tris-buffered saline (TBS) (150 mM sodium chloride, 2 mM Tris base, pH 7.4) containing 0.1 % Tween20 (Sigma) (TBS-T). Blocked membranes were probed for SMAD2 (1:1000, Cell Signalling Technology 5339S), pSMAD2 (1:1000, Cell Signalling Technology 18338S), SMAD1 (1:1000, Cell Signalling Technology 6944S), pSMAD1/5/9 (1:1000, Cell Signalling Technology 13820S), Tubulin (1:1000, Cell Signalling Technology 2148S), primary antibodies diluted in 5 % milk/TBS-T (w/v) overnight at 4 °C. Membranes were then washed for 15 min and 3 × 5 min in TBS-T buffer and stained with anti-mouse HRP (1:4000, Cell Signalling Technology 7076S) or anti-rabbit HRP (1:4000, Cell Signalling Technology 7074S) secondary antibodies for 1 h at RT. Membranes were treated with Pierce ECL+ blotting substrate (Thermo Scientific 32,132) for 5 min. Images were obtained using Thermofisher's MyECL machine. Protein levels were quantified using ImageJ and normalised to the signal area of tubulin.

4.12. Statistical analysis

Statistical analysis carried out as per figure legends using GraphPad Prism 8™ software.

CRediT authorship contribution statement

HD, LYY isolated and characterised the pericytes from microtia patients. YX performed the AFM and XPS. LL performed the super resolution miscroscopy. HD, AK and LYY performed the experiments. HD, YX analysed the data. HD, AK, LYY, CCW, MJD devised experiments. CCW, MSS and MJD supervised the research. HD and MJD wrote the manuscript. All authors revised the manuscript.

Table 1
Primers for qRT-PCR.

Target	Primer sequence
B-Actin	5′- CCAGAGGCGTACAGGGATAG −3′ 5′- CCAACCGCGAGAAGATGA −3′
COL2A	5’-CACTGGGACTGTCCTCTGCGA-3′ 5’-CCTTTGGTCCTGGTTGCCCACT-3′
ALP	5’-CTTGGCTTTTCCTTCATGGT-3′ 5’-AGAACCCCAAAGGCTTCTTC-3′
COLX	5′-CACCTTCTGCACTGCTCATC-3′ 5′-GGCAGCATATTCTCAGATGGA-3′

Declaration of competing interest

The authors declare the following financial interests/personal relationships which may be considered as potential competing interests: Manuel Salmeron-Sanchez has patent MATERIALS AND METHODS FOR TISSUE REGENERATION pending to University of Glasgow. Co-author is Editor-in-Chief of Biomaterials Advances - MSS.

Data availability

Data will be made available on request.

Acknowledgements

This work was supposed by EPSRC grant (EP/P001114/1). LYY and CWW was supported by a Royal College of Surgeons Edinburgh pump priming grant (SPPG/17/112) and a grant from the William Rooney Plastic Surgery and Burns Research Trust. We would also like to thank F Rossi and C Cryer (SCRM Flow Cytometry Facilities) for technical assistance with fluorescence activated cell sorting (FACS) and flow cytometry.

Appendix A. Supplementary data

Supplementary data to this article can be found online at https://doi.org/10.1016/j.bioadv.2023.213370.

References

[1] British Academy of Audiology, British Association of Audiovestibular Physicians, British Association of Paediatricians in Audiology, British Association of Plastic Reconstructive and Aesthetic & Surgeons. n.d. UK Care Standards for the Management of Patients With Microtia and Atresia. https://www.ndcs.org.uk/document.rm?id=10317 (2015).
[2] N. Baluch, et al., Auricular reconstruction for microtia: a review of available methods, Can. J. Plast. Surg. 22 (2014) 39–43.
[3] A. Rodriguez, et al., Characteristics of cartilage engineered from human pediatric auricular cartilage, Plast. Reconstr. Surg. 103 (1999) 1111–1119.
[4] S.J. Shieh, S. Terada, J.P. Vacanti, Tissue engineering auricular reconstruction: in vitro and in vivo studies, Biomaterials 25 (2004) 1545–1557.
[5] L. Nayyer, M. Birchall, A.M. Seifalian, G. Jell, Design and development of nanocomposite scaffolds for auricular reconstruction. Nanomedicine nanotechnology, Biol. Med. 10 (2014) 235–246.
[6] L. Nayyer, et al., Tissue engineering: revolution and challenge in auricular cartilage reconstruction, Plast. Reconstr. Surg. 129 (2012) 1123–1137.
[7] J. Xue, et al., Engineering ear-shaped cartilage using electrospun fibrous membranes of gelatin/polycaprolactone, Biomaterials 34 (2013) 2624–2631.
[8] H. Kusuhara, et al., Tissue engineering a model for the human ear: assessment of size, shape, morphology, and gene expression following seeding of different chondrocytes, Wound Repair Regen. 17 (2009) 136–146.
[9] A. Haisch, Ear reconstruction through tissue engineering, Adv. Otorhinolaryngol. 68 (2010) 108–119.
[10] Y. Cao, J.P. Vacanti, K.T. Paige, J. Upton, C.A. Vacanti, Transplantation of chondrocytes utilizing a polymer-cell construct to produce tissue-engineered cartilage in the shape of a human ear, Plast. Reconstr. Surg. 100 (1997) 297–304.
[11] L. Zhou, et al., Engineering ear constructs with a composite scaffold to maintain dimensions, Tissue Eng. - Part A 17 (2011) 1573–1581.
[12] L. Zhang, et al., Regeneration of human-ear-shaped cartilage by co-culturing human microtia chondrocytes with BMSCs, Biomaterials 35 (2014) 4878–4887.
[13] S. Landau, et al., Human-engineered auricular reconstruction (hEAR) by 3D-printed molding with human-derived auricular and costal chondrocytes and adipose-derived mesenchymal stem cells, Biofabrication 14 (2022).

[14] J. Lee, E. Lee, H. Kim, Y. Son, Comparison of articular cartilage with costal cartilage in initial cell yield, degree of dedifferentiation during expansion and redifferentiation capacity, Biotechnol. Appl. Biochem. 48 (2007) 149.
[15] B. Ma, et al., Gene expression profiling of dedifferentiated human articular chondrocytes in monolayer culture, Osteoarthr. Cartil. 21 (2013) 599–603.
[16] A.J. Reiffel, et al., High-Fidelity tissue engineering of patient-specific auricles for reconstruction of pediatric microtia and other auricular deformities, PLoS One 8 (2013).
[17] M.F.Bin Ishak, et al., The formation of human auricular cartilage from microtic tissue: Aan in vivo study, Int. J. Pediatr. Otorhinolaryngol. 79 (2015) 1634–1639.
[18] A.O. Oseni, P.E. Butler, A.M. Seifalian, Optimization of chondrocyte isolation and characterization for large-scale cartilage tissue engineering, J. Surg. Res. 181 (2013) 41–48.
[19] T. Takahashi, et al., Synergistic effects of FGF-2 with insulin or IGF-I on the proliferation of human auricular chondrocytes, Cell Transplant. 15 (2006) 367.
[20] S.H. Kamil, A. Rodriguez, C.A. Vacanti, R.D. Eavey, M.P. Vacanti, Expansion of the number of human auricular chondrocytes: recycling of culture media containing floating cells, Tissue Eng. 10 (2004) 139–144.
[21] H. Yanaga, K. Imai, Y. Tanaka, K. Yanaga, Two-stage transplantation of cell-engineered autologous auricular chondrocytes to regenerate chondrofat composite tissue: clinical application in regenerative surgery, Plast. Reconstr. Surg. 132 (2013) 1467–1477.
[22] M.F. Pittenger, et al., Multilineage potential of adult human mesenchymal stem cells, Science (80-.) 284 (1999) 143–147.
[23] R.A. Somoza, J.F. Welter, D. Correa, A.I. Caplan, Chondrogenic differentiation of mesenchymal stem cells: challenges and unfulfilled expectations, Tissue Eng. - Part B Rev. 20 (2014) 596–608.
[24] K. Pelttari, et al., Premature induction of hypertrophy during in vitro chondrogenesis of human mesenchymal stem cells correlates with calcification and vascular invasion after ectopic transplantation in SCID mice, Arthritis Rheum. 54 (2006) 3254–3266.
[25] K. Liu, et al., The dependence of in vivo stable ectopic chondrogenesis by human mesenchymal stem cells on chondrogenic differentiation in vitro, Biomaterials 29 (2008) 2183–2192.
[26] Y. Yang, et al., Mesenchymal stem cell-derived extracellular matrix enhances chondrogenic phenotype of and cartilage formation by encapsulated chondrocytes in vitro and in vivo, Acta Biomater. 69 (2018) 71–82.
[27] O. Ghali, et al., Dexamethasone in osteogenic medium strongly induces adipocyte differentiation of mouse bone marrow stromal cells and increases osteoblast differentiation, BMC Cell Biol. 16 (2015) 1–15.
[28] L. Bian, D.Y. Zhai, R.L. Mauck, J.A. Burdick, Coculture of human mesenchymal stem cells and articular chondrocytes reduces hypertrophy and enhances functional properties of engineered cartilage, Tissue Eng. - Part A 17 (2011) 1137–1145.
[29] F. Long, Building strong bones: molecular regulation of the osteoblast lineage, Nat. Rev. Mol. Cell Biol. 13 (2012) 27–38.
[30] M. Crisan, et al., A perivascular origin for mesenchymal stem cells in multiple human organs, Cell Stem Cell 3 (2008) 301–313.
[31] E.V. Alakpa, et al., Improving cartilage phenotype from differentiated pericytes in tunable peptide hydrogels, Sci. Rep. 7 (2017) 1–11.
[32] E.V. Alakpa, et al., Tunable supramolecular hydrogels for selection of lineage-guiding metabolites in stem cell cultures /j.Chempr.2016.07.001)), Chem 1 (2016) 512.
[33] C.L. Esteves, F.X. Donadeu, Pericytes and their potential in regenerative medicine across species, J. Int. Soc. Adv. Flow Cytom. (2017), https://doi.org/10.1002/cyto.a.23243.
[34] M.T. Rojewski, B.M. Weber, H. Schrezenmeier, Phenotypic characterization of mesenchymal stem cells from various tissues, Transfus. Med. Hemother. 35 (2008) 168–184.
[35] M.J. Dalby, A.J. García, M. Salmeron-Sanchez, Receptor control in mesenchymal stem cell engineering, Nat. Rev. Mater. 3 (2018) 17091.
[36] V. Llopis-hernández, et al., Material-driven fibronectin assembly for high-efficiency presentation of growth factors, Sci. Adv. 1–11 (2016), https://doi.org/10.1126/sciadv.1600188.
[37] Z.A. Cheng, et al., Nanoscale coatings for ultralow dose BMP-2-driven regeneration of critical-sized bone defects, Adv. Sci. 1800361 (2018) 1800361.
[38] M. Bieniek, V. Llopis-Hernandez, K. Douglas, M. Salmeron-Sanchez, C. Lorenz, Minor chemistry changes alter surface hydration to control fibronectin adsorption and assembly into nanofibrils, Adv. Theory Simul. 1900169 (2019) 1–13.
[39] A. Alba-Perez, V. Jayawarna, P.G. Childs, M.J. Dalby, M. Salmeron-Sanchez, Plasma polymerised nanoscale coatings of controlled thickness for efficient solid-phase presentation of growth factors, Mater. Sci. Eng. C 113 (2020), 110966.
[40] M. Cantini, P. Rico, D. Moratal, M. Salmerón-Sánchez, Controlled wettability, same chemistry: biological activity of plasma-polymerized coatings, Soft Matter 8 (2012) 5575–5584.
[41] J.F. Watts, Book review: high-resolution XPS of organic polymers: the scienta ESCA300 database, Surf. Interface Anal. 20 (1993), 145-145.
[42] M.M. Martino, et al., Engineering the growth factor microenvironment with fibronectin domains to promote wound and bone tissue healing, Sci. Transl. Med. 3 (2011) 100ra89.
[43] M.M. Martino, J.A. Hubbell, The 12th-14th type III repeats of fibronectin function as a highly promiscuous growth factor-binding domain, FASEB J. 24 (2010) 4711–4721.
[44] S.L. Dallas, et al., Fibronectin regulates latent transforming growth factor-β (TGFβ) by controlling matrix assembly of latent TGFβ-binding protein-1, J. Biol. Chem. 280 (2005) 18871–18880.
[45] Y. Xiao, et al., Material-driven fibronectin and vitronectin assembly enhances BMP-2 presentation and osteogenesis, Mater. Today Bio 16 (2022), 100367.
[46] A.I. Monteiro, T. Kollmetz, J. Malmström, Engineered systems to study the synergistic signaling between integrin-mediated mechanotransduction and growth factors (Review), Biointerphases 13 (2018), 06D302.
[47] M. Salmerón-Sánchez, M.J. Dalby, Synergistic growth factor microenvironments, Chem. Commun. 52 (2016) 13327–13336.
[48] C. Margadant, A. Sonnenberg, Integrin-TGF-B crosstalk in fibrosis, cancer and wound healing, EMBO Rep. 11 (2010) 97–105.
[49] T.F. Li, R.J. O'Keefe, D. Chen, TGF-beta signaling in chondrocytes, Front. Biosci. 10 (2005) 681–688.
[50] R.N. Wang, et al., Bone morphogenetic protein (BMP) signaling in development and human diseases, Genes Dis. 1 (2014) 87–105.
[51] B.P. Cohen, J.L. Bernstein, K.A. Morrison, J.A. Spector, L.J. Bonassar, Tissue engineering the human auricle by auricular chondrocyte-mesenchymal stem cell co-implantation, PLoS One 13 (2018) 1–19.
[52] N. Kang, et al., Effects of co-culturing BMSCs and auricular chondrocytes on the elastic modulus and hypertrophy of tissue engineered cartilage, Biomaterials 33 (2012) 4535–4544.
[53] J. Fischer, A. Dickhut, M. Rickert, W. Richter, Human articular chondrocytes secrete parathyroid hormone-related protein and inhibit hypertrophy of mesenchymal stem cells in coculture during chondrogenesis, Arthritis Rheum. 62 (2010) 2696–2706.
[54] M. Wang, et al., Trophic stimulation of articular chondrocytes by late-passage mesenchymal stem cells in coculture, J. Orthop. Res. 31 (2013) 1936–1942.
[55] J.-F. Gilles, et al., DiAna, an ImageJ tool for object-based 3D co-localization and distance analysis, Methods (2016), https://doi.org/10.1016/j.ymeth.2016.11.016ï.